# Pedestal Characterization and Stability of Small-ELM Regimes in NSTX

A. Sontag 1), J. Canik 1), R. Maingi 1), J. Manickam 2), P. Snyder 3), R. Bell 2), S. Gerhardt 2), S. Kubota 4), B. LeBlanc 2), D. Mueller 2), T. Osborne 3), K. Tritz 5)

1) Oak Ridge National Laboratory, Oak Ridge, TN, USA
2) Princeton Plasma Physics Laboratory, Princeton, NJ, USA
3) General Atomics, San Diego, CA, USA
4) University of California Los Angeles, Los Angeles, CA, USA
5) John's Hopkins University, Baltimore, MD, USA

E-mail contact of main author: sontagac@ornl.gov

**Abstract**. An instability near the plasma edge known as the edge harmonic oscillation (EHO) is thought to enable access to the ELM-free quiescent H-mode (QH-mode) in tokamaks, which is a highly desirable operational regime for ITER because of the avoidance of periodic ELM heat loads. The EHO has been hypothesized to be a saturated kink driven unstable by toroidal rotational shear that provides sufficient transport near the plasma edge to keep the edge plasma below the peeling-ballooning stability limit. NSTX has observed unstable modes with similar characteristics to the EHO coincident with transition to a small-ELM regime (called Type-V). These small ELMs do not have a measurable effect on the plasma stored energy (< 1%). Transition to this regime is associated with a downward biased plasma as evidenced by drsep < -5 mm. Soft x-ray emission indicates that these modes are localized just inside the pedestal and are correlated with increased density fluctuations in the pedestal as measured by microwave reflectometry. The lowest order mode rotates at the plasma rotation frequency, indicating n=1, and harmonics up to n=6 have been observed simultaneously with the n=1, as determined by the rotation frequency of the higher harmonics. Increased edge collisionality is required to access Type-V ELMs. Stability analysis during the observed modes indicates instability to n=1-3 with n=3 having the highest growth rate and unstable mode eigenfunctions peaked near the plasma edge. Discharges with Type-V and Type-I ELMs are both calculated to be on the peeling unstable side of the peeling-ballooning stability curve, with the Type-V case at higher normalized pressure gradient.

## 1. Introduction

Predictable and reliable access to H-mode regimes with small or no ELMs is highly desirable for future large experiments such as ITER to ensure adequate survivability of the first wall [1]. At standard aspect ratio, one such operating regime, the quiescent H-mode (QH-mode), has been observed on DIII-D [2], ASDEX [3], JT-60U [4], and JET [3]. The QH-mode has not been observed in low aspect ratio ST experiments, although a small-ELM operating regime (called Type-V ELMs) has been observed on NSTX [5,6] that may have similar origins to the QH-mode.

Access to QH-mode has been linked to the appearance of an MHD instability near the plasma edge called the edge harmonic oscillation, or EHO [7]. The EHO allows access to the QH-mode by providing necessary transport near the edge to stabilize the peeling-ballooning modes responsible for ELMs [8], while maintaining good core confinement inside the pedestal. NSTX has observed transition to a small-ELM operating regime where each ELM

has less than a 1% impact on the plasma stored energy [5]. The transition to this regime is correlated with the appearance of low-frequency (<10 kHz) MHD oscillations near the plasma edge that have similar characteristics to the EHO. The EHO is hypothesized to be a saturated low-n kink that is destabilized by rotational shear and is accessed at low density and high rotational shear at the plasma edge [8,9]. The conditions required to access the edge instability in NSTX and the effects of this mode on transport will be examined and compared to the EHO.

This paper will discuss the characteristics of the observed NSTX instability in Section 2. Section 3 will cover the plasma conditions that are observed when the mode is present, including MHD stability properties. The paper will conclude with a discussion of whether the mode is required to access the small-ELM operational regime in Section 4.

## 2. Edge Mode Characteristics

The time evolution of an NSTX discharge with a transition to small-ELMs and the associated edge instability is shown in Figure 1. In this discharge, there are some large ELMs after the plasma current flat-top, then a transition to small-ELMs occurs at 0.29 s as shown in the $D_\alpha$ trace in panel (b). The small-ELMs decrease the plasma stored energy by < 1%, i.e. well below the statistical uncertainty in equilibrium reconstructions. In NSTX discharges, transition to the small-ELM regime is associated with a downward biased plasma as evidenced by $\delta_r^{sep} < -5$ mm, which is consistent with previous observations [5] ($\delta_r^{sep}$ is the radial separation of the two separatraces at the outer midplane).
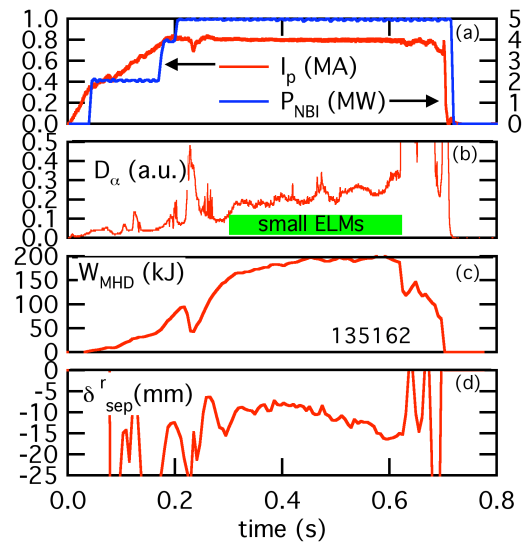
*Figure 1: Time evolution of shot 135162 showing a transition to small-ELMs at 0.29 s. Shown are: (a) toroidal plasma current ($I_p$) and injected neutral beam power ($P_{NBI}$), (b) emission intensity of the deuterium alpha spectral line ($D_\alpha$), (c) plasma stored magnetic energy ($W_{MHD}$), and (d) the radial separation of the two separatraces at the outboard midplane. ($\delta^r_{sep}$).*

The edge mode coincident with the transition to small ELMs is observed in the B-dot coils as well as in Ultrasoft X-ray (USXR) emission [10], as shown in panels (a) and (b) of Figure 2. The channels of the diode array have lines of sight at a single toroidal location that extend

from the magnetic axis into the scrapeoff layer. The diodes are filtered with 10 μm of Be foil, which eliminates low energy radiation from the scrape-off layer and lower pedestal.

The mode is observed as low frequency oscillations that grow strongly in two channels near the plasma edge starting at approximately 0.29s (coincident with the transition to small-ELMs). These oscillations are coherent with a frequency of 1-3 kHz. This frequency is the same as the measured toroidal rotation frequency at the radius where the mode amplitude peaks, indicating an n=1 instability. Toroidal mode analysis of the fundamental mode observed on the Mirnov coils also indicates n = 1.

The oscillations observed on the USXR array initially appear to grow in-phase, indicative of an ideal perturbation, as shown in Figure 3. This figure shows the time evolution of the four USXR channels nearest the edge for shot 135162, filtered to a frequency window of 500 Hz – 80 kHz. Channel 12 has a line of sight that passes very near the top of the pedestal with lower channel numbers corresponding to views closer to the magnetic axis. The observed mode amplitude peaks near the plasma edge and decreases in the channels viewing closer to the magnetic axis. The mode is not observed in channels closer to the magnetic axis than channel 9. The mode is also not observed in channel 13, which views the scrape-off layer. In some cases, an inversion is observed between channels 11 and 12 at later times (50 -100 ms after the initial mode appearance), but this phenomenon is not universal. These oscillations persist throughout the small-ELM period. After 0.5 s, multiple harmonics can be observed with frequencies corresponding to integer multipliers of the lowest frequency mode, which is similar to observations of the EHO.
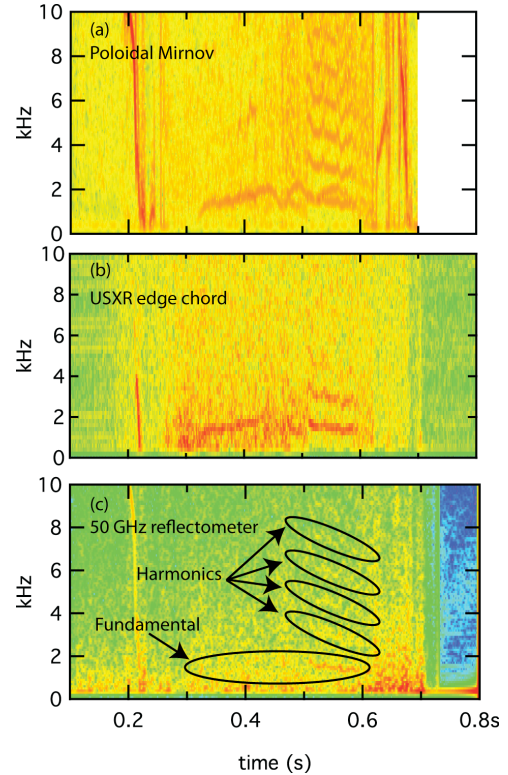


*Figure 2: Measurements of an instability near the plasma edge in shot 135162 including (a) a Poloidal Mirnov coil, (b) a USXR chord viewing near the plasma edge, and (c) a reflectometer channel with a cutoff location near the top of the pedestal.*
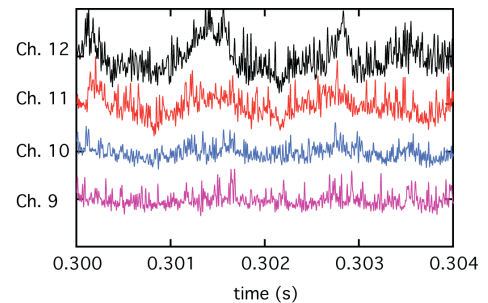


*Figure 3: USXR diode array signals in 4 channels viewing near the plasma edge with 10 μm Be filters and frequency filtered to 0.5 – 80 kHz. Channel 12 has a line of sight near the top of the pedestal, with decreasing channels viewing closer to the magnetic axis.*

Reflectometer measurements with the cutoff frequency near the top of the pedestal, as shown in Figure 2(c), show density fluctuations at the same frequencies as the observed modes. Initial TRANSP [11] modeling of discharges both with and without the edge mode show little to no difference in the single-fluid effective transport coefficient near the edge, as shown in Figure 4. It should be noted that the TRANSP modeling does not account for particle sources and sinks at the plasma edge, so there is great uncertainty outside of $\rho_{pol} = 0.85$. These two discharges have similar time evolution of most global parameters, and their characteristics are discussed in greater detail in Section 3. More detailed modeling, including particle sources and sinks is required to determine if this instability is providing the particle transport required to stabilize the peeling-ballooning modes, as is suspected with the EHO.



*Figure 4: Single fluid effective transport coefficient for two shots, one with large Type-I ELMs (red) and one with small Type-V ELMs (black).*

## 3. Plasma Characteristics and MHD Stability

A comparison of two similar discharges, one with large Type-I ELMs and one with small Type-V ELMs, illustrates the advantages of operating in a small-ELM regime and provides an opportunity to determine the plasma conditions required for a transition to this regime. The time evolution for two shots with similar time evolution of global plasma parameters, except for a programmed change in triangularity at 0.3 s, is shown in Figure 5. The control discharge (135155) has large Type-I ELMs throughout the discharge, while the second discharge (135159) transitions to a small-ELM regime soon after the decrease in triangularity. The edge mode discussed in
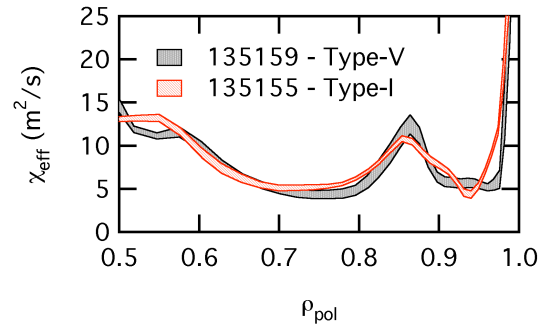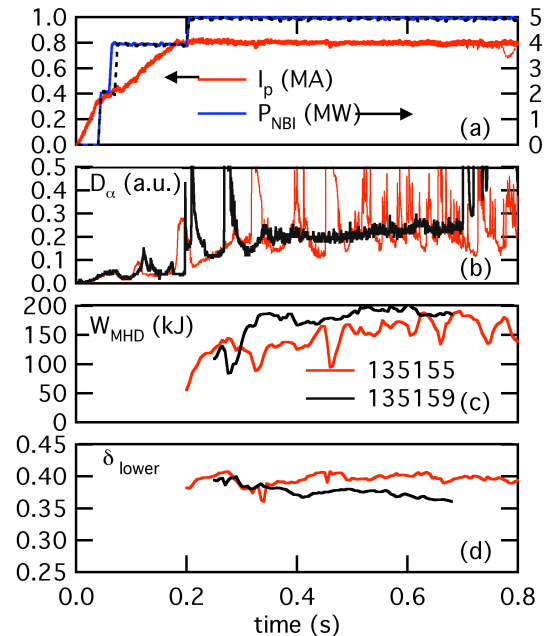


*Figure 5: Time evolution of two discharges with similar global plasma parameters but different ELM characteristics. The control shot (red) has Type-I ELMs. The second shot (black) transitions to a small-ELM regime coincident with a programmed change in triangularity at 0.3 s.*

Section 2 is observed in the small-ELM discharge but not in the control discharge. The small-ELM discharge has higher stored energy, without the large fluctuations that occur during the Type-I ELM crashes. The location of the plasma boundary is also more stable and the edge temperature and density profiles are relatively stationary in the Type-V case, without the cycle of edge pressure buildup and crash associated with Type-I ELMs.

An edge profile comparison using single time point measurements of the Thomson scattering [12] and CHERS [13] diagnostics has been performed for these two shots to determine if the change in profile characteristics going from Type-I to Type-V ELMs are similar to those associated with access to QH-mode and the EHO at standard aspect ratio. The time for the profile comparison was chosen to be during the small-ELM time for the Type-V discharge and between ELMs at 50% of the ELM cycle for the Type-I discharge. The edge electron pressure and pressure gradient for these two discharges are shown in Figure 6. The small-ELM discharge has a reduced peak pedestal pressure gradient, as seen in Figure 6 (b), and a less distinct pedestal top which is shifted inward by approximately 2 cm, as shown in Figure 6 (a). These two qualities are in general stabilizing to peeling-ballooning modes, however detailed stability calculations are still required to determine the plasma stability to these modes.

A comparison of the edge rotation, rotation shear and collisionality between these two shots is shown in Figure 7. Shot 135155 has slightly increased rotation (Figure 7 (a)) but decreased rotation shear near the top of the pedestal (Figure 7 (b)) as compared to the small-ELM discharge, which is
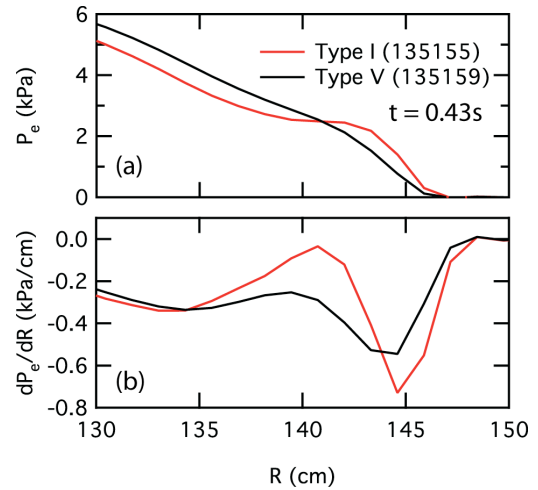


Figure 6: Comparison of (a) electron pressure profile and (b) electron pressure profile gradient at 0.43 s for discharges with Type I (red) and Type V (black) ELMs.
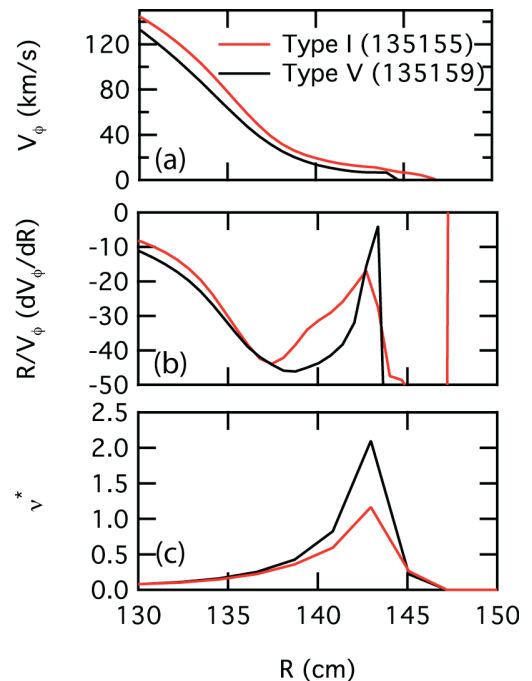


Figure 7: Comparison of (a) toroidal rotation profile, (b) toroidal rotation shear, and (c) normalized collisionality, $v^*$, for discharges with Type I (red) and Type V (black) ELMs. The top of the pedestal is at R = 143 cm for both discharges.

consistent with increased rotation shear resulting in destabilization of the edge mode. Analysis of a larger database of shots shows a wide variation in both rotation and rotation shear at the top of the pedestal for Type-I and Type-V discharges, so these results are not conclusive. The small-ELM discharge shows increased edge collisionality, consistent with past observations of Type-V ELMs as compared to Type-I ELMing discharges [5]. Analysis of a larger database of shots indicates that $v^* > 1$ at the top of the H-mode pedestal eliminates Type-I ELMs in NSTX, leaving only Type-V. The Type-V discharges also show a general trend of increased pedestal pressure as compared to Type-I discharges.

The peeling mode is an edge-localized, current-driven external kink, so increased pedestal collisionality associated with Type-V ELMs hints that the mode might be stabilized by the reduction in the pressure-driven current near the edge. The current profiles for these discharges were determined using a procedure developed on DIII-D [8,14] and briefly outlined here: 1) Reconstruct the MHD equilibrium at the times of Thomson scattering measurements using the EFIT [15] code with magnetic diagnostics for constraint. 2) Map the $n_e$, $T_e$ and $n_i$ profiles into normalized flux space. 3) Fit a modified hyperbolic tangent function [16] to the aggregate profile data from a specified time window. 4) Compute the equilibrium using the fit profiles as additional constraints. The Sauter neoclassical model [17] then provides an estimate of the edge bootstrap current.



*Figure 8: Reconstructed edge current profiles for two discharges. One with Type-I ELMs (red) and one with Type-V ELMs (black)*

The profile from the Type-I discharge was determined by averaging plasma properties over a time window from 0.4 - 0.55 s and restricting the data to points in the last 50% of the ELM cycle. All time points in the same time window were used for the Type-V discharge. Figure 8 shows a comparison of the reconstructed total toroidal current profiles for these two discharges. The case with small ELMs shows a slight reduction in the peak current from the Type-I case.
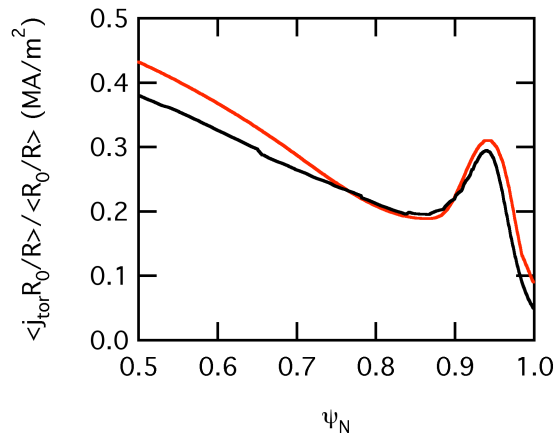
Ideal MHD stability analysis using these profiles has been performed using both the ELITE [18,19] and PEST [20] stability codes. PEST calculations indicate n = 3-5 are the most

unstable modes, with the mode eigenfunctions peaking near the plasma edge. Figure 9 shows the ELITE peeling-ballooning stability calculations for n=3,6,9,12 and 15 in the Type-I case. The red region in the upper left portion of the figure represents the unstable portion of the stability space. The stability boundary of $\gamma/(\omega_*/2) = 0.1$ is consistent with the calculated ELM stability of previous NSTX discharges [21]. This case is on the boundary that denotes the peeling side of the stability curve with n = 3 being the most unstable mode. Being on the peeling side of the stability curve is typical for NSTX discharges due to the strong bootstrap current drive at low aspect ratio as compared to standard aspect ratio. The high shaping of NSTX discharges is stabilizing to ballooning modes [22], which results in the ballooning stability boundary being off the right hand side of Figure 9.
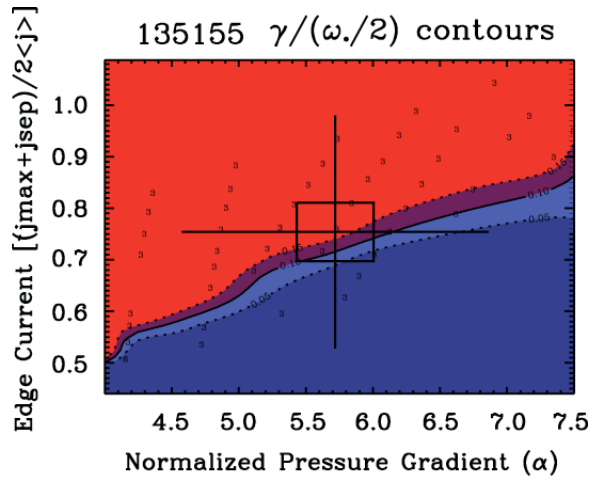


Figure 9: Peeling-ballooning stability diagram as calculated by the ELITE code for shot 135155 during the Type-I ELMy phase.
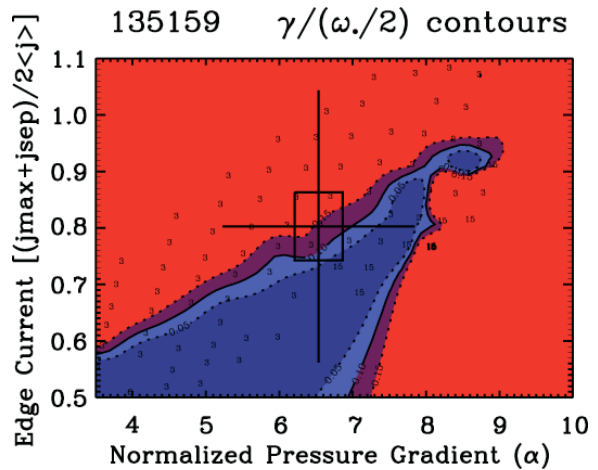


Figure 10: Peeling-ballooning stability diagram as calculated by the ELITE code for shot 135159 during the Type-V ELMy phase.

Figure 10 shows the peeling-ballooning stability calculation for the same toroidal modes in the Type-V ELMy case. The plasma is still in the unstable region on the peeling side of the stability curve, however, the decreased triangularity (Figure 5(d)) has decreased the stability to ballooning modes. This results in the appearance of the ballooning boundary on the right-hand side of the figure. The most unstable mode is again n = 3, but the operating point is now quite close to the n=15 stability boundary, due to the decreased ballooning stability. Similar stability calculations for DIII-D show that discharges with the EHO lie near to but on the stable side of the peeling stability boundary [8,9]. In DIII-D discharges, the operating point moves to decreased edge current and pressure gradient when going from Type-I to QH-mode. In contrast, the change from Type-I to Type-V ELMs in NSTX is accompanied by a transition to higher pressure gradient.

**4. Summary and Discussion**

The presence of an edge instability has been correlated with the transition to a small-ELM operating regime in NSTX. The mode has characteristics similar to the EHO, and is localized near the top of the pedestal. Density fluctuations due to this instability have been measured, but initial transport modeling is unable to determine if this instability is providing increased edge transport to stabilize the peeling-ballooning modes responsible for Type-I ELMs.

The transition to small-ELMs is also correlated to increased $v^*$ near the edge. This is in contrast to the QH-mode, which is accessed at decreased $v^*$. Comparison of two discharges that have differing ELM characteristics show that the edge current is slightly decreased in the small-ELM case, but both cases are calculated to be on the unstable side of the peeling boundary with the Type-V case having higher pressure gradient. Decreased triangularity in the Type-V case brings this discharge closer to the ballooning stability boundary than is typically observed in NSTX, though further analysis is required to determine if this change in operating point is related to the transition to Type-V ELMs.

[1] J. Roth, *et. al*., *J. Nucl. Mater*. **1** (2009) 390.
[2] C.M. Greenfield, *et al.*, *Phys. Rev. Lett.* **86** (2001) 4544.
[3] W. Suttrop, *et al., Nucl. Fusion* **45** (2005) 721.
[4] Y. Sakamoto *et al., Plasma Phys. Control. Fusion* **46** (2004) A299.
[5] R. Maingi, *et al.*, *Nucl. Fusion* **45** (2005) 264.
[6] R. Maingi, *et al.*, *Phys. Plasmas* **13** (2006) 092510.
[7] K.H. Burrell, *et al.*, *Phys. Plasmas* **8** (2001) 2153.
[8] P.B. Snyder, *et al., Nucl. Fusion* **47** (2007) 961.
[9] K.H. Burrell, *et al.*, *Nucl. Fusion* **49** (2009) 085024.
[10] D. Stutman, *et al.*, *Rev. Sci. Instrum.* **74** (2003) 1982.
[11] J. Ongena, *et al.*, *Trans. Fusion Technol.* **33** (1998) 181.
[12] B.P. LeBlanc, *et al.*, *Rev. Sci. Instrum.* **74** (2003) 1659.
[13] R.E. Bell, *et al.*, *Bull. Am. Phys. Soc.* **48** (2003) 217 LP1 25.
[14] T.H. Osborne, *et al.*, *J. Phys. Conf. Ser.* **123** (2008) 012014.
[15] L.L. Lao, *et al., Nucl. Fusion* **25** (1985) 1611.
[16] R.J. Groebner and T.H. Osborne, *Phys. Plasmas* **5** (1998) 1800.
[17] O. Sauter, *et al., Phys. Plasmas* **6** (1999) 2834.
[18] H.R. Wilson, *et al.*, *Phys. Plasmas* **9** (2002) 1277.
[19] P.B. Snyder, *et al.*, *Phys. Plasmas* **9** (2002) 2037.
[20] R. Grimm, *et al.*, *Methods of Comp. Phys.* **16** (1976) 253.
[21] R. Maingi, *et al.*, *Phys. Rev. Lett.* **103** (2009) 075001.
[22] P.B. Snyder, *et al., Plasma Phys. Control. Fusion* **46** (2004) A131.